

Reset dynamics and latching in niobium superconducting nanowire single-photon detectors

Anthony J. Annunziata,^{1,a)} Orlando Quaranta,^{2,3} Daniel F. Santavicca,¹ Alessandro Casaburi,^{2,3} Luigi Frunzio,^{1,2} Mikkel Ejnraes,² Michael J. Rooks,¹ Roberto Cristiano,² Sergio Pagano,⁴ Aviad Frydman,⁵ and Daniel E. Prober¹

¹Department of Applied Physics, Yale University, New Haven, Connecticut 06511, USA

²Istituto di Cibernetica “E. Caianiello,” CNR, 80078 Pozzuoli, Italy

³Dipartimento di Fisica “E. R. Caianiello,” Università di Salerno, 84081 Baronissi, Italy

⁴Dip. Matematica e Informatica and CNR-SPIN Salerno, Università di Salerno, 84084 Fisciano, Italy

⁵Department of Physics, Bar-Ilan University, 52520 Ramat Gan, Israel

(Received 29 June 2010; accepted 30 August 2010; published online 22 October 2010)

We study the reset dynamics of niobium (Nb) superconducting nanowire single-photon detectors (SNSPDs) using experimental measurements and numerical simulations. The numerical simulations of the detection dynamics agree well with experimental measurements, using independently determined parameters in the simulations. We find that if the photon-induced hotspot cools too slowly, the device will latch into a dc resistive state. To avoid latching, the time for the hotspot to cool must be short compared to the inductive time constant that governs the resetting of the current in the device after hotspot formation. From simulations of the energy relaxation process, we find that the hotspot cooling time is determined primarily by the temperature-dependent electron-phonon inelastic time. Latching prevents reset and precludes subsequent photon detection. Fast resetting to the superconducting state is, therefore, essential, and we demonstrate experimentally how this is achieved. We compare our results to studies of reset and latching in niobium nitride SNSPDs.

© 2010 American Institute of Physics. [doi:10.1063/1.3498809]

I. INTRODUCTION

Superconducting nanowire single-photon detectors (SNSPDs) offer high detection efficiency for visible and near infrared photons with high count rates, very small timing jitter, and low dark count rates.^{1–5} Typical detectors consist of a current-biased superconducting niobium (Nb), niobium nitride (NbN), or niobium titanium nitride (NbTiN) nanowire patterned into a meander, as seen in Fig. 1(a). In this meander geometry, the nanowire length is proportional to the detection area. SNSPDs are particularly useful in applications that require high count rate single-photon detection in the near infrared, such as photon-counting communication⁶ and quantum key distribution.⁷ Development of NbN SNSPDs is most advanced. Although NbN SNSPDs offer higher count rates than most other near infrared single-photon detectors,⁸ the count rate in large area meander devices is limited by the kinetic inductance of the nanowire, which is proportional to the nanowire length. For a small-area detector (short nanowire), the count rate can be higher, but very short nanowires will latch into a finite voltage state instead of self-resetting to the superconducting state after detecting a photon. Latching precludes practical use of a small-area SNSPD at high count rate.

The count rate in a properly resetting SNSPD is set by the electrical time constant $\tau_r = L_K/R_L$, where L_K is the kinetic inductance of the nanowire, proportional to its length, and R_L is the load resistance of the readout circuit.⁹ Before a photon is absorbed, the nanowire is superconducting with dc

bias current I_b that is less than the critical current at the base temperature, I_{c0} . An absorbed photon will create a localized hotspot in the nanowire, which has a finite resistance R_d that drives the bias current into the load resistance R_L . The equivalent circuit for a device with a finite resistance hotspot is seen in Fig. 1(b). In the desired mode of operation, the SNSPD will self-reset to the superconducting state. This occurs because the hotspot cools quickly after the current is shunted out of the nanowire, so that R_d abruptly returns to zero. The device current $I_d(t)$ then exponentially returns to its initial value before photon absorption, I_b , with a time constant of τ_r . The equivalent circuit for this current return stage

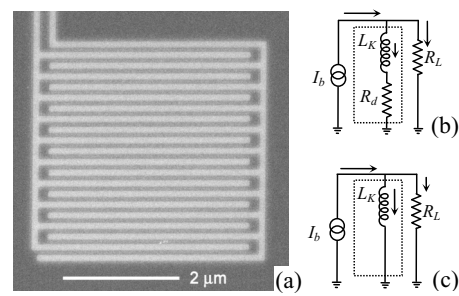


FIG. 1. (a) Scanning electron micrograph of a meandered Nb SNSPD with a detection area of $16 \mu\text{m}^2$. The dark regions are Nb, while the sapphire substrate is lighter. (b) Equivalent circuit for the nanowire and readout with a photon-induced hotspot resistance R_d . Prior to photon absorption, $R_d=0$ and I_b flows fully through L_K . The nanowire is outlined by the dotted box; the arrows indicate the flow of current. (c) Equivalent circuit as the bias current is returning to the device after the hotspot has cooled back to the zero-resistance state. For this stage, the inductive time constant of this circuit, L_K/R_L , sets the time scale for reset of the detector, which characterizes the decay of the load current toward zero.

^{a)}Electronic mail: ajannunz@us.ibm.com.

is shown in Fig. 1(c). Full reset requires a time of approximately $3\tau_r$ so that $I_d(t)$ will be restored to approximately 95% of I_b . This is necessary in order to have a high probability of detecting the next photon that is absorbed in the nanowire.¹⁰ The maximum count rate is, therefore, the reciprocal of this full reset time, $\approx(3\tau_r)^{-1}$. The reset time can be reduced by increasing R_L (Refs. 10 and 11) or decreasing L_K .^{12–15} If τ_r is too small, however, the device will not self-reset but instead will latch into a finite voltage state where it is not sensitive to photons.^{10,11,16}

In this article, we study the reset and latching dynamics of Nb SNSPDs using both experiments and numerical simulations. We compare these results to our measurements of NbN SNSPDs, and to those of other groups.^{1–4,9–11} Reset and latching have previously been studied in NbN SNSPDs.¹¹ The present study is the first to examine the reset and latching dynamics in Nb SNSPDs.¹¹ A Nb SNSPD has less kinetic inductance than a NbN SNSPD of the same geometry; however, Nb has a longer electron-phonon time than NbN. As will be shown, the kinetic inductance and the electron-phonon time both play a significant role in determining the reset dynamics, which makes this comparison instructive. This work should be relevant to understanding the limits on the count rates of SNSPDs made from other materials^{5,15,16}. The present work also explains our previously reported experimental results for Nb SNSPDs.^{17,18}

II. BACKGROUND

The stability of self-heating hotspots in superconducting wires has been broadly studied and several models have been presented.^{10,11,19–21} Reference 11 studied the phenomenon of latching in NbN SNSPD devices in detail. The analysis in Ref. 11 uses a phenomenological model of the heating and cooling of the photon-created resistive hotspot to determine if an NbN SNSPD will latch. According to Ref. 11, electro-thermal feedback creates a situation where a resistive hotspot is either stable or unstable in the steady-state, depending on I_b and τ_r . Formation of a stable hotspot, known as latching, precludes operation of the SNSPD. Thus, in the case of the SNSPD, parameters that give unstable hotspot behavior are desired.

Solutions to the model in Ref. 11 were obtained analytically by determining the stability of the hotspot under small sinusoidal perturbations. This type of small-signal stability analysis does not model the time-dependent formation, evolution, and decay of the hotspot. The predictions of the model in Ref. 11 were fit to data from NbN SNSPDs. By varying several of the phenomenological parameters of the model, good agreement between the model predictions and experimental data was found. However, some of the phenomenological parameters used in Ref. 11, notably the “hotspot temperature stabilization time,” are not directly connected to the microscopic physical processes, such as electron-phonon scattering, phonon-escape and electron diffusion. These physical processes govern energy relaxation in superconducting thin films, and are important for understanding other nonequilibrium superconducting devices such as hot electron bolometers and transition edge sensors.^{22,23}

Identifying which of these physical processes plays the key role in the SNSPD is important. Additionally, in Ref. 11, the values of some parameters that are obtained by the fitting procedure appear to be different from those of independent measurements.^{16–18,22–27} For example, the results in Ref. 11 based on fitting imply a value of the thermal conductivity κ in NbN of approximately 0.0017 W/K m. Direct measurements of the thermal conductivity in NbN, and calculations based on the Wiedemann–Franz law, have obtained $\kappa \approx 0.16$ W/K m.¹⁰ We do believe that the model in Ref. 11 provides guidance that is useful in understanding trends within the data presented, and also may capture physical effects occurring at the superconducting-normal interface of the hotspot that may be particularly important to understand latching in NbN SNSPDs, with their higher resistivity and shorter length normal-superconducting interfaces.

In the present work, we develop a model to analyze latching in Nb SNSPDs based on microscopic physical processes. These are well-known to govern thermal relaxation in superconducting thin films and nanowires. A photon-created hotspot can stabilize to either a finite resistance or cool back to zero-resistance. The factors that determine whether or not a hotspot will latch are identified by examining the full dynamics of the hotspot formation and how the dynamics depend on I_b , L_K , and R_L . We find that almost all of the energy stored in the kinetic inductance of the nanowire, $(1/2)L_KI_b^2$, is dissipated into the hotspot as Joule heat when the hotspot forms. This inductive energy dissipation occurs over a time scale that is significantly less than 1 ns in most Nb devices. We conclude that this total inductive energy determines whether a device will latch for a specific value of the current return time $\tau_r=L_K/R_L$. The predictions of our model agree well with measurements of Nb SNSPDs with no free parameters. The parameters used in our model are based on independent measurements.

We find that Nb SNSPDs are significantly more susceptible to latching than NbN devices because cooling by phonon emission in Nb is much slower than in NbN. Although this slower cooling is less desirable for high count rate operation, it makes Nb a good material in which to study latching. The conclusions we draw from our model of Nb SNSPDs should be applicable to SNSPDs fabricated from other materials as well. We also tested NbN devices to verify that our measurement methods did not introduce any spurious behavior in our measurements of Nb SNSPDs. Proper shielding, filtering, and clean, low noise microwave design are critical to these measurements. Our measured results for NbN are similar to those reported in Ref. 11, confirming the validity of our measurements.

III. DEVICES TESTED

The fabrication procedures for the Nb and NbN devices measured in this work are described in Refs. 18 and 24, respectively. A summary of the parameters of the devices tested is given in Table I. Both Nb and NbN devices were fabricated by etching of sputter-deposited thin films on R-plane sapphire substrates. The Nb nanowires were ≈ 7.5 nm thick and 100 nm wide. The critical temperature T_c of the

TABLE I. Parameters of the devices studied in this work. The sheet resistance R_s is measured approximately 5 K above T_c . The reported values of the kinetic inductance for each device in the table include approximately 10 nH of inductance from the measurement leads (Ref. 29).

	Nb (A) $10 \times 10 \mu\text{m}^2$	Nb (B) $4 \times 4 \mu\text{m}^2$	Nb (C) 10 μm line	NbN (D) $5 \times 5 \mu\text{m}^2$	NbN (E) 5 μm line
Length, L	500 μm	80 μm	10 μm	105 μm	5 μm
R_s (Ω/sq)	110	116	113	890	895
T_c	4.5 K	3.9 K	4.0 K	10 K	10 K
I_c (1.7 K)	8.2 μA	6.2 μA	6.4 μA	26.2 μA	25.4 μA
L_K (1.7 K)	235 nH	60 nH	15 nH	120 nH	16 nH

Nb devices ranged from 3.9 to 4.5 K. We attribute this variation in T_c to small variations in the thickness of the samples, which are correlated with small variations ($\sim 5\%$) in the sheet resistance of the nanowires just above T_c . This thickness variation may affect the superconductivity strongly because the nanowires are very thin.¹⁵ We believe that the variation in thickness is a result of the nonuniformity of the Nb etching process used.¹⁸ Based on the measured temperature dependence of the critical current, the variation in T_c can explain the variation in the critical currents of the Nb devices measured at 1.7 K. All NbN nanowires were ≈ 5 nm thick, 130 nm wide and $\approx 900 \Omega/\text{sq}$ just above T_c . The critical temperature of the NbN devices was consistently 10 K for the devices tested. The small difference in the critical current between the two devices presented here may be due to small, nongeometric constrictions in the nanowires that are not visible in scanning electron micrograph images. This variation is consistent with what is observed in Ref. 11 for unconstricted NbN devices. All devices studied in this work had good ($\sim 5\%$) detection efficiency for 470 nm photons and uniform line width. No large constrictions were apparent in measurements of the current versus voltage, measurements of the detection efficiency, or in measurements of the kinetic inductance.²⁵ The devices studied were chosen from a larger group of devices, some of which did contain significant non-geometric constrictions, as discussed in Ref. 25. The detection efficiency of all devices tested can likely be improved significantly by using optical structures designed to increase the absorption in the Nb film, as was demonstrated for NbN SNSPDs in Ref. 4.

The measurement setup is described in Ref. 18 and an equivalent circuit is given in Fig. 2(a). A key feature of the experimental setup is a set of cryogenic, remote-controlled rf switches. These enable measurement during one cool down of a given device with various shunt resistors in parallel with the transmission line but close to the device. This gives total load resistances $R_L=50$ (with no shunt), 33, 25 (with a 50 Ω shunt), 17, or 15 Ω . For devices with small inductance, a small load resistance is necessary to enable self-resetting operation, as will be explained. We measured L_K independently by incorporating each device into an LC resonant circuit with known capacitance and measuring the resonant frequency $= (L_K C)^{-1/2}$, for a range of temperatures below T_c and for a range of currents below I_{co} using a network analyzer. The technique used is described in detail in Ref. 28 and is different from the technique used in Ref. 9. The measured values of L_K at 1.7 K are reported in Table I for $I_b=0$. The dependence of L_K on I_b is weak, varying by $\approx 5\%$ in Nb nanowires

as I_b is increased to just below I_c . The kinetic inductance measurements are discussed in detail in Ref. 28.

IV. MODEL

The simulations we have performed are based on numerical solutions to a two-temperature model of heat flow similar to the model used to analyze NbN SNSPDs in Ref. 20. In two-dimensions, the governing equations of the model are

$$\begin{aligned} T_e = & -\frac{1}{\tau_{e-ph}(T_e)}(T_e - T_{ph}) + \frac{1}{C_e(T_e)}j_d(x,y,t)^2\rho_d(x,y,t) \\ & + D_e\nabla^2 T_e, \end{aligned} \quad (1)$$

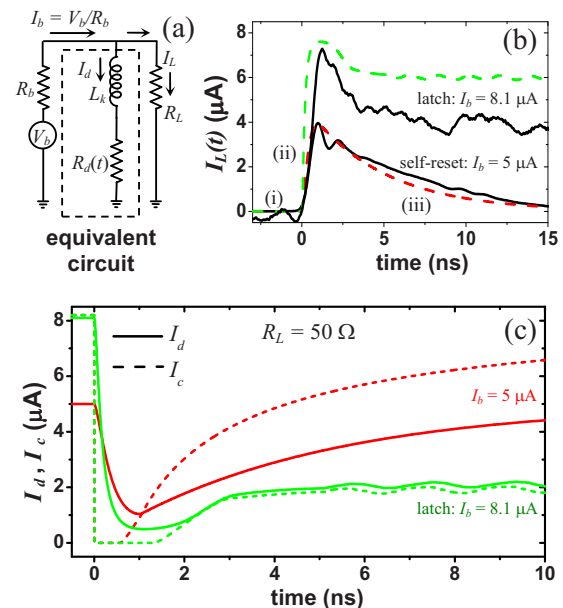


FIG. 2. (Color online) (a) Equivalent circuit; $R_b \gg R_L$, R_d . (b) Measured (solid lines) and simulated (dashed lines) output pulses, $I_L(t)$, for device (A) with the self-resetting case labeled by the three regimes of operation: (i) the device is in equilibrium with $R_d=0$; (ii) initial heating: a photon has been absorbed, the hotspot is growing and the current is transferring into the load; (iii) the hotspot resistance has returned to zero, and the current is returning to the device with a time constant $\tau_r=L_K/R_L$. (c) Numerical results for $I_c(t)$ (dashed lines) and $I_d(t)=I_b-I_L(t)$ (solid lines) for $I_b=5.0$ (upper curve) and 8.1 μA (lower curve); the latter shows the latching case. We find $I_{\text{latch}}=7.1 \mu\text{A}$ from these simulations. We note that I_c as defined here can be finite even with $R_d>0$ because I_c is calculated according to Eq. (7) and, therefore, only depends on the electron temperature, and not on I_d . R_d is calculated from the simulation according to Eq. (6).

$$\dot{T}_{ph} = \frac{1}{\tau_{e-ph}(T_e)} \frac{C_e(T_e)}{C_{ph}(T_{ph})} (T_e - T_{ph}) - \frac{1}{\tau_{esc}} (T_{ph} - T_o) + D_{ph} \nabla^2 T_{ph}, \quad (2)$$

where $T_e = T_e(x, y, t)$ and $T_{ph} = T_{ph}(x, y, t)$, are the electron and phonon temperatures, T_o is the substrate temperature, $\tau_{e-ph}(T_e)$ is the electron-phonon inelastic scattering time, τ_{es} is the escape time for phonons (equal to 40 ps in all simulations),²³ D_e and D_{ph} are the electron and phonon diffusivities, $C_e(T_e)$ and $C_{ph}(T_{ph})$ are the heat capacities of the electrons and phonons per unit volume, $j_d(x, y, t)$ is the current density, and $\rho_d(x, y, t)$ is the resistivity. In all simulations of Nb SNSPDs, we use $\tau_{e-ph}(T_e) = \tau_{e-ph}(6.5 \text{ K})(6.5 \text{ K}/T_e)^2$ with $\tau_{e-ph}(6.5 \text{ K}) = 2.0 \text{ ns}$,²³ $D_e = 1 \text{ cm}^2/\text{s}$,²⁷ $D_{ph} = 0.1 \text{ cm}^2/\text{s}$, and $C_{ph}(T_{ph}) = 9.8 \times 10^{-6} T_{ph}^3 (\text{J}^* \text{cm}^{-3} \text{K}^{-1})$.^{10,30} For the electronic heat capacity, in the normal state we use $C_{eN}(T_e) = 5.8 \times 10^{-2} T_e (\text{J}^* \text{cm}^{-3} \text{K}^{-1})$,²⁷ and in the superconducting state we use $C_{eS}(T_e) = 0.92^* \exp(-\Delta(T_e)/k_B T_e) \times (\text{J}^* \text{cm}^{-3} \text{K}^{-1})$,^{27,29-31} where $\Delta(T_e) = 1.76 k_B T_c^* (1 - T_e/T_c)^{1/2}$.³⁰

The total current flowing through the device, $I_d(t)$, is determined by the readout circuit [Fig. 2(a)] and, therefore, obeys the equation

$$\dot{I}_d(t) = -\frac{1}{L_K} [R_d(t) + R_L] I_d(t) + R_L \frac{I_b}{L_K}, \quad (3)$$

which is obtained using Kirchhoff's laws, where $R_d(t)$ is the resistance of the nanowire and $I_b = V_b/R_b$ in Fig. 2(a). The spatial distribution of the current density $j_d(x, y, t)$ is determined by the spatially-dependent resistivity $\rho_d(x, y, t)$. If the coordinate system is oriented such that the positive x -axis is along the length of the nanowire in the direction of current flow, the total device current at position (x) for a wire of width w , and thickness d much smaller than the magnetic penetration depth, is given by

$$I_d(t) = I_d(x, t) = d \int_0^w j_d(x, y, t) dy, \quad (4)$$

which, by conservation of charge, must be equal at all points (x). The local resistivity $\rho_d(x, y, t)$ will depend on the whether the point (x, y) in the material is in the superconducting or the normal (nonsuperconducting) state. In our model, the resistivity is defined by

$$\rho_d(x, y, t) = \rho_o [1 - \{H[T_c - T_e(x, y, t)] \\ \times H[j_c - j_d(x, y, t)]\}], \quad (5)$$

where H is the Heaviside step function and ρ_o is the normal state resistivity of the film. Thus, $\rho_d(x, y, t)$ is equal to zero or ρ_o , depending on temperature and current density. Since only those sections of the strip at point (x) that are normal for all values of (y) at (x) will contribute to R_d , it follows that for a wire of width w ,

$$R_d(t) = \frac{l_{\text{norm}}(t)}{dw} \rho_o, \quad (6)$$

where the normal length $l_{\text{norm}}(t)$ is calculated numerically and is the length over which the resistive hotspot occupies

the entire width of the wire. Typically, the maximum value of l_{norm} is much less than the total nanowire length l . Finally, we calculate the effective critical current of the device as a function of time, $I_c(t)$. The effective critical current is defined as the minimum critical current along the length of the nanowire using the Ginzburg-Landau expression for the temperature dependence

$$I_c(t) = \min_x \left\{ d \int_0^w j_c(T_e=0) \left[1 - \frac{T_e(x, y, t)}{T_c} \right]^{3/2} dy \right\}, \quad (7)$$

with $j_c(T_e=0)$ determined for each device by equating the Ginzburg-Landau expression for $I_c(1.7 \text{ K}) = I_c(T_e=0)(1 - 1.7/T_c)^{3/2}$ to measurements of $I_c(1.7 \text{ K})$ and setting $j_c = I_c/wd$.³¹ As defined, the effective critical current is assumed to be independent of I_d . Since the effective critical current is only determined by temperature, once the hotspot begins to cool below the critical temperature, $I_c(t)$ becomes a measure of the thermal relaxation of the highest temperature region of the hotspot. Thus, the time scale over which the critical current returns to near its equilibrium value is the hotspot thermal relaxation time τ_c . This is the time required for hot electrons to return to near their equilibrium temperature T_o .

We have implemented a numerical solution to these equations using MATLAB.³² The device is represented by a two-dimensional grid with longitudinal grid spacing Δx and transverse grid spacing Δy . At each grid point, the electron and phonon temperatures are defined. From these temperatures, all temperature-dependent quantities are defined. When a volume-dependent quantity such as the heat capacity is calculated, it is calculated over the volume of the cell centered at the grid point (x, y) where the volume of the cell is equal to $d\Delta x \Delta y$ with typical grid spacing of $\Delta x = \Delta y = 5 \text{ nm}$. The absorption of a photon is simulated by increasing the temperature of one grid point in one time step Δt such that

$$T_e(x_o, y_o) = T_o + \frac{hf}{C_e(T_o) \cdot (\Delta x \Delta y)}, \quad (8)$$

where (x_o, y_o) is the grid point where the photon is absorbed, h is Planck's constant, and f is the frequency of the photon.

V. RESULTS

The detection cycle in an SNSPD, as illustrated by the simulations, can be divided into three distinct stages, labeled on the lower curve in Fig. 2(b): (i) the nanowire is biased in the superconducting state with a dc bias current I_b below the critical current at the base temperature, $I_{co} = I_c(T_o)$; here, $R_d = 0$. (ii) A photon creates a resistive hotspot whose resistance $R_d(t)$ increases quickly due to the fast dissipation of the inductive energy stored in L_K . As a result, most of I_b is shunted into R_L , which has much lower resistance than R_d . (iii) In a self-resetting device, after most of the bias current has transferred to R_L , the hotspot quickly returns to the zero-resistance state and the current slowly begins to transfer back into the device with a return time constant $\tau_r = R_L/L_K$. In a latching device, stages (i) and (ii) are identical to those in a self-resetting device, however stage (iii) does not occur and

R_d remains finite. Latching is seen in Fig. 2(b) for $I_b = 8.1 \mu\text{A}$. As will be shown next, latching occurs in this device ($L_K=235 \text{ nH}$ and $R_L=50 \Omega$) at the larger value of I_b because of the greater heating that occurs due to the larger amount of stored inductive energy, $\approx(1/2)L_KI_b^2$, that is dissipated in the hotspot. If the hotspot does not cool quickly enough as the current begins to return to the device, the device will remain in (latch into) the resistive state. The measured latching pulse in Fig. 2(b) is for a single shot measurement. It has more noise than the measured self-resetting pulse because the self-resetting waveform displayed is an average of many pulses. The measured slow decay of $I_L(t)$ in the latching case for $t > 5 \text{ ns}$ is due to the ac coupling of the amplifier. This slow decay is not observed in the simulation, which assumes a dc-coupled amplifier.

It is essential that I_b be close to I_{co} for high detection efficiency.²⁰ Thus, self-reset for $I_b \leq I_c$ is necessary for a device to have both a high count rate and high detection efficiency. In Fig. 2(c), we model the effect of increasing I_b from 5 to $8.1 \mu\text{A}$ by computing both the effective time-dependent critical current $I_c(t)$ and the device current $I_d(t)$ as functions of time. The fast dissipation of the inductive energy, $(1/2)L_KI_b^2$, that occurs after the photon is absorbed drives I_c quickly to zero [Fig. 2(c)] and R_d to a large value. This large value of R_d drives I_d to near zero because I_b is shunted almost entirely into the lower resistance load, R_L . This entire process occurs in a very short time, $<1 \text{ ns}$ in most devices, as observed from the rise time of the current pulses in Fig. 2(b). The cooling time in Nb is much longer than the sub-nanosecond time to dissipate the inductive energy, $(1/2)L_KI_b^2$.

Self-reset occurs when the trajectories of $I_c(t)$ and $I_d(t)$ are such that $I_d(t) < I_c(t)$ as the hotspot cools. For device (A) with $R_L=50 \Omega$, Fig. 2(c) shows that self-reset occurs for $I_b = 5 \mu\text{A}$ but not for $I_b = 8.1 \mu\text{A}$. When $I_b = 8.1 \mu\text{A}$, $I_d(t)$ remains above $I_c(t)$ as the hotspot begins to cool, maintaining a finite hotspot resistance. The resulting dc Joule heating (occurring after the initial energy dissipation) enforces a stable, finite resistance hotspot state. The resistance of this stable state may be less than the peak resistance of the hotspot, which occurs just after the fast initial dissipation of the inductive energy and before any substantial cooling has taken place. Note in Fig. 2(c) for $I_b = 8.1 \mu\text{A}$ that the finite value of I_c for long times indicates that the steady-state temperature at the center of the hotspot is less than T_c ; nevertheless, the hotspot remains resistive because $I_d > I_c$. We define a latching current I_{latch} as the lowest value of I_b that results in latching. For device (A) in Fig. 2 with $R_L=50 \Omega$ the model predicts that $I_{\text{latch}} = 7.1 \mu\text{A}$. Note that in Fig. 2(c), the current return time is $\approx 4.6 \text{ ns}$, close to the expected value of $L_K/R_L = 4.7 \text{ ns}$.

We now show that our numerical simulations agree with experimental measurements. In Fig. 3, we plot the normalized latching current measured for several Nb SNSPDs versus $\tau_r = L_K/R_L$. We also plot predictions for the latching current obtained by simulating devices with the same parameters as those measured. In addition to the measurements and simulations for Nb devices, we also plot experimental measurements of the latching current in NbN devices

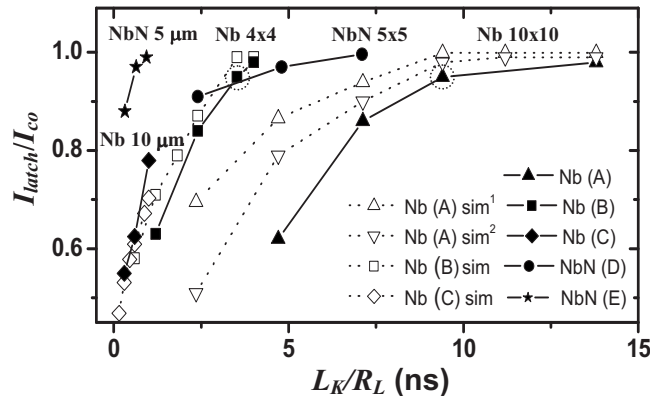


FIG. 3. Normalized latching current predicted by the model (open symbols) and measured (solid symbols) vs $\tau_r = L_K/R_L$, obtained by varying R_L in the simulations and experiments. For the $10 \times 10 \mu\text{m}^2$ meander, we plot predictions for two values of the diffusion constant: $D_e = 1 \text{ cm}^2/\text{s}$, as used in all other simulations, and $D_e = 0.25 \text{ cm}^2/\text{s}$, which is used only here.

to provide a comparison of the two different materials. Each device has a different value of L_K (see Table I). We vary R_L to change τ_r in both simulations and experiments. For Nb device (A), we plot predictions for two values of D_e (1.0 and $0.25 \text{ cm}^2/\text{s}$) to show that faster diffusion of hot electrons (larger D_e) makes a device less susceptible to latching. A value of $D_e = 1.0 \text{ cm}^2/\text{s}$ was used for all other Nb simulations. The simulation predictions for Nb SNSPDs and the experimental measurements of Nb SNSPDs are in approximate quantitative agreement. In the simulations, there are no free fitting parameters used. We believe the discrepancies between simulated and measured values of I_{latch} are primarily due to uncertainty in the values of the material parameters used as inputs to the model.^{10,23,27,29,30}

We find in experiments that a Nb SNSPD is much more sensitive to latching than a NbN SNSPD with the same area and value of R_L . Still, we observe that NbN SNSPDs are also susceptible to latching, as discussed in Ref. 11. A trend we observe for both Nb and NbN devices is that with larger kinetic inductance, a larger value of τ_r is required to achieve the same normalized value of I_{latch} . For larger L_K , the dissipated energy $\approx(1/2)L_KI_b^2$ is larger. For example, in Fig. 3 the circled data points for devices (A) and (B) are both at $I_{\text{latch}} = 0.95I_c$; device (A) has $L_K = 235 \text{ nH}$, $R_L = 25 \Omega$, and $\tau_r = 9.4 \text{ ns}$ while device (B) has $L_K = 60 \text{ nH}$, $R_L = 17 \Omega$, and $\tau_r = 3.5 \text{ ns}$.

From simulations, we find that latching occurs when the current return time τ_r is significantly shorter than the hotspot cooling time τ_c . We define τ_c as the time interval between when $I_c(t)$ first becomes finite and when $I_c(t) = 0.63I_{co}$ (see Fig. 3). This criterion allows us to compare τ_r to τ_c . Simulations show that τ_c depends on material parameters (e.g. the electron-phonon time) as well as on the inductive energy $(1/2)L_KI_b^2$. After photon absorption and the fast dissipation of the inductive energy, the hotspot temperature is significantly greater than the equilibrium temperature T_o . The maximum temperature is greatest for the largest inductive energy. We find from simulations of Nb SNSPDs that the temperature-dependent electron-phonon interaction time in Nb is the dominant component of τ_c but not the only component. For

small temperature excursions, τ_c would be equal to the electron-phonon time,²² $\tau_{e-ph}(T_e) \propto T_e^{-2}$. However, for the large temperature changes that occur in an SNSPD, the thermal relaxation has a more complex behavior than simple exponential relaxation and also depends on $R_d(t)$ and on the outdiffusion of hot electrons. Thus, simulations are needed to predict the exact trajectories of $I_c(t)$ and $I_d(t)$, and therefore, if a device will latch or self-reset.

Simulations confirm that the inductive energy dissipation in the hotspot occurs on a time scale much shorter than τ_c and can be much larger than the energy of the photon that initiates the hotspot. From simulations, we find that the exact energy dissipated in the hotspot as it is forming is equal to $=(1/2)L_K(I_b^2 - I_{min}^2) + hf$, where I_{min} is the minimum value of I_d and hf is the energy of the absorbed photon, where h is Planck's constant and f is the frequency of the photon. For most practical devices (large area and, therefore, large L_K), $hf \ll (1/2)L_KI_b^2$. In all measurements and simulations, we find that $I_{min} \ll I_b$, so that the total initial dissipated energy is approximately equal to the inductive energy $(1/2)L_KI_b^2$ for all but the shortest nanowires [e.g. device (C), where the photon energy hf is significant]. In a self-resetting device, the total amount of energy dissipated in a detection event is this initially dissipated energy, $(1/2)L_KI_b^2$, since the hotspot quickly cools back to near T_o and $R_d=0$ after the inductive energy is dissipated. In a latching device, $I_d(t)$ remains above $I_c(t)$ as the hotspot begins to cool. In this case, the hotspot remains resistive as I_d begins to increase, causing additional Joule heating after the inductive energy is dissipated. This additional Joule heating enforces a stable dc hotspot resistance.

The hotspot size, and hence the resistance, is determined primarily by the energy stored in the kinetic inductance. If two hotspots are formed simultaneously at different locations along the nanowire, the total energy dissipated in both hotspots will be $\approx (1/2)L_KI_b^2$. This will result in a combined resistance of the two hotspots that is approximately equal to the resistance of an individual hotspot. Hence, it is not feasible to distinguish a single-photon detection event from a multiphoton detection event via a measurement of the peak height in a conventional SNSPD, even if the amplifier impedance were comparable to the hotspot resistance.

In all devices, a larger value of $(1/2)L_KI_b^2$ leads to a hotspot with a greater peak temperature. This increases the cooling time τ_c since more energy must be transferred to the phonon system and ultimately to the substrate in order for the hotspot to cool to near T_o . Since $(1/2)L_KI_b^2$ and τ_c are both independent of R_L , we can reduce R_L in order to increase τ_c without affecting the cooling time τ_c . We can, therefore, eliminate latching in any device by sufficiently reducing R_L . However, reducing R_L decreases the count rate, proportional to $(3\tau_c)^{-1}$ and reduces the output signal, $\approx I_bR_L$.

In Fig. 4, we show the effects of changing L_K and I_b for four different situations. We plot simulations of $R_d(t)$ and $I_c(t)$ for Nb devices with $R_L=25 \Omega$. (Note that in Fig. 2, $R_L=50 \Omega$ was used.) The inductive energy is varied by changing L_K (compare device B with $L_K=60 \text{ nH}$ to device C with $L_K=15 \text{ nH}$) and by changing I_b [compare device (A) with $I_b=5 \mu\text{A}$ to device (A) with $I_b=8.19 \mu\text{A}$]. The plots of the simulated data clearly show that the peak value of R_d

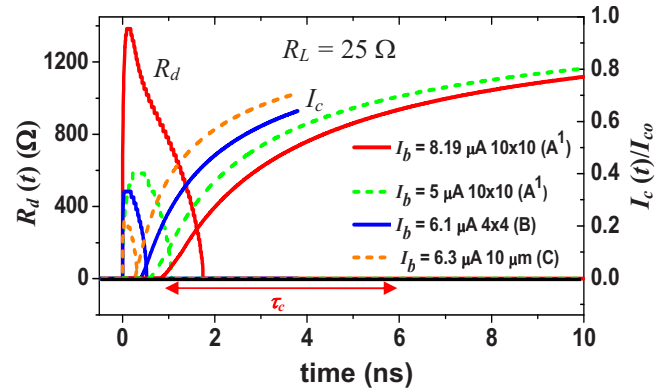


FIG. 4. (Color online) : Simulation results for Nb devices (A), (B), and (C) showing the dependence of $R_d(t)$ and $I_c(t)$ on I_b and L_K ; $R_L=25 \Omega$; and τ_c is labeled for device (A) with $I_b=8.19 \mu\text{A}$ and is equal to 5.0 ns. For device (C), $\tau_c=2.2$ ns (not labeled).

as well as the value of the cooling time τ_c increases for larger values of $(1/2)L_KI_b^2$. For example, in Fig. 4, τ_c increases from 2.2 to 5.0 ns when the value of $(1/2)L_KI_b^2$ is increased from 5 eV for device (C) to 85 eV for device (A) with $I_b=8.19 \mu\text{A}$ and $hf=2.6$ eV in these simulations.

In addition to circuit parameters, the thermal relaxation process also depends on material parameters. In particular, the cooling time τ_c decreases when the electron-phonon time is decreased. Also, if D_e is increased, τ_c decreases due to faster outdiffusion of hot electrons [see device (A) in Fig. 3 where two values of D_e are considered]. The dependence of τ_c on these material parameters likely explains the difference in the observed latching behavior between Nb and NbN SNSPDs (Fig. 3). NbN has a much shorter electron-phonon time than Nb at all relevant temperatures.²⁶ This makes NbN less prone to latching because the shorter electron-phonon time more than compensates for the smaller D_e and the larger value of $(1/2)L_KI_b^2$ in NbN compared to Nb of similar geometry.

VI. CONCLUSION

We have demonstrated that our microscopic model of the electron heating and cooling can predict the observed reset and latching behavior in a Nb SNSPD. Our simulations and measurements of Nb SNSPDs show behavior qualitatively similar to our measurements of NbN SNSPDs and to the results reported in Ref. 11 for NbN SNSPDs. In Nb SNSPDs, we find that the fast initial heating caused by the Joule dissipation of the energy stored in the kinetic inductance of the nanowire determines whether a device will latch or self-reset. In Nb, latching occurs over a wider range of operating parameters than for NbN SNSPDs. This is due to the much longer electron-phonon time in Nb. Our model suggests that the maximum count rate for an Nb SNSPD would be for a device with small L_K [e.g., device (C)]. The maximum count rate then is $(3\tau_{c,min})^{-1} \approx 150$ MHz. The factor of three is necessary so that the current in the nanowire is restored to greater than 95% of its initial, dc value, which enables a high detection probability for the next photon that is absorbed. To achieve this count rate with device (C), a value of $R_L \approx 7 \Omega$ would be required (see Fig. 3), which was not avail-

able in our measurement setup. We do demonstrate that in a larger area Nb SNSPD [device (A)], a value of $R_L=25\ \Omega$ is sufficient to achieve the maximum count rate (see Fig. 3). The maximum count rate for device A with $R_L=25\ \Omega$ is $(3 \times 235\text{ nH}/25\ \Omega)^{-1}=36\text{ MHz}$ because L_K is much larger than in device (C) and, therefore, much more heating occurs. We find that the intrinsic timescale for cooling of the hot electrons is the electron-phonon inelastic time. This sets the minimum reset time of an SNSPD. Thus, reducing the kinetic inductance helps only insofar as it reduces the inductive energy that is dissipated as the hotspot forms, which reduces the cooling time. Based on this conclusion, a NbTiN SNSPD, with a smaller kinetic inductance than a NbN SNSPD of the same geometry,¹⁵ may have some advantages over NbN SNSPDs if the electron-phonon inelastic times are similar. However, even if an SNSPD were fabricated from a superconducting material with a shorter electron-phonon time than NbN, such as MgB₂, the phonon-escape time τ_{es} probably cannot be reduced significantly from its value for ultrathin NbN, where $\tau_{es} \approx 40\text{ ps}$.³³ Recently, new geometries that incorporate several nanowires in parallel have been explored.^{34,35} The added degrees of freedom for the current in these parallel topologies may allow for faster reset than a single nanowire of the same detection area.

ACKNOWLEDGEMENTS

This work was supported by NSF under Grant Nos. ECS-0622035 and DMR-0907082 and an NSF Graduate Research Fellowship to one of us (A.J.A.).

- ¹G. Gol'tsman, O. Minaeva, A. Korneev, M. Tarkov, I. Rubtsova, A. Divochiy, I. Milostnaya, G. Chulkova, N. Kaurova, B. Voronov, D. Pan, J. Kitaygorodsky, A. Cross, A. Pearlman, I. Komissarov, W. Slysz, M. Wegrzeczk, P. Grabiec, and R. Sobolewski, *IEEE Trans. Appl. Supercond.* **17**, 246 (2007).
- ²J. A. Stern and W. H. Farr, *IEEE Trans. Appl. Supercond.* **17**, 306 (2007).
- ³A. D. Semenov, P. Haas, B. Gunther, H. W. Hubers, K. Il'in, M. Siegel, A. Kirste, J. Beyer, D. Drung, T. Schurig, and A. Smirnov, *Supercond. Sci. Technol.* **20**, 919 (2007).
- ⁴K. M. Rosfjord, J. K. W. Yang, E. A. Dauler, A. J. Kerman, V. Anant, B. M. Voronov, G. Gol'tsman, S. A. Hamilton, and K. K. Berggren, *Opt. Express* **14**, 527 (2006).
- ⁵S. N. Dorenbos, E. M. Reiger, U. Perinetti, V. Zwiller, T. Zijlstra, and T. M. Klapwijk, *Appl. Phys. Lett.* **93**, 131101 (2008).
- ⁶B. S. Robinson, A. J. Kerman, E. A. Dauler, D. M. Boroson, S. A. Hamilton, J. K. W. Yang, V. Anant, and K. K. Berggren, *Proc. SPIE* **6709**, 67090Z (2007).
- ⁷R. H. Hadfield, J. L. Habif, J. Schlafer, R. E. Schwall, and S. W. Nam, *Appl. Phys. Lett.* **89**, 241129 (2006).
- ⁸R. H. Hadfield, *Nat. Photonics* **3**, 696 (2009).
- ⁹A. J. Kerman, E. A. Dauler, W. E. Keichler, J. K. W. Yang, K. K. Berggren, G. Gol'tsman, and B. Voronov, *Appl. Phys. Lett.* **88**, 111116 (2006).
- ¹⁰J. K. W. Yang, A. J. Kerman, E. A. Dauler, V. Anant, K. M. Rosfjord, and K. K. Berggren, *IEEE Trans. Appl. Supercond.* **17**, 581 (2007).
- ¹¹A. J. Kerman, J. K. W. Yang, R. J. Molnar, E. A. Dauler, and K. K. Berggren, *Phys. Rev. B* **79**, 100509 (2009).
- ¹²M. Ejrnaes, R. Cristiano, O. Quaranta, S. Pagano, A. Gaggero, F. Mattioli, R. Leoni, B. Voronov, and G. Gol'tsman, *Appl. Phys. Lett.* **91**, 262509 (2007).
- ¹³M. Ejrnaes, A. Casaburi, R. Cristiano, O. Quaranta, S. Marchetti, and S. Pagano, *J. Mod. Opt.* **56**, 390 (2009).
- ¹⁴M. Tarkov, J. Claudon, J. P. Poizat, A. Korneev, A. Divochiy, O. Minaeva, V. Seleznev, N. Kaurova, B. Voronov, A. V. Semenov, and G. Gol'tsman, *Appl. Phys. Lett.* **92**, 241112 (2008).
- ¹⁵S. Miki, M. Takeda, M. Fujiwara, M. Sasaki, A. Otomo, and Z. Wang, *Appl. Phys. Express* **2**, 075002 (2009).
- ¹⁶C. Portesi, S. Borini, E. Taralli, M. Rajteri, and E. Monticone, *Supercond. Sci. Technol.* **21**, 034006 (2008); H. Shibata, T. Maruyama, T. Akazaki, H. Takesue, T. Honjo, and Y. Tokura, *Physica C* **468**, 1992 (2008).
- ¹⁷A. J. Annunziata, D. F. Santavicca, J. D. Chudow, L. Frunzio, M. J. Rooks, A. Frydman, and D. E. Prober, *IEEE Trans. Appl. Supercond.* **19**, 327 (2009).
- ¹⁸A. J. Annunziata, A. Frydman, M. O. Reese, L. Frunzio, M. Rooks, and D. E. Prober, *Proc. SPIE* **6372**, 63720V (2006).
- ¹⁹W. Skocpol, M. R. Beasley, and M. Tinkham, *J. Appl. Phys.* **45**, 4054 (1974).
- ²⁰A. Semenov, P. Haas, H. W. Hübers, K. Il'in, M. Siegel, A. Kirste, D. Drung, T. Schurig, and A. Engel, *J. Mod. Opt.* **56**, 345 (2009).
- ²¹K. S. Il'in, M. Lindgren, M. Currie, A. D. Semenov, G. N. Gol'tsman, R. Sobolewski, S. I. Cherednichenko, and E. M. Gershenson, *Appl. Phys. Lett.* **76**, 2752 (2000).
- ²²P. J. Burke, R. J. Schoelkopf, A. Skalare, B. Karasik, M. C. Gaidis, W. R. McGrath, B. Bumble, H. G. LeDuc, and D. E. Prober, *J. Appl. Phys.* **85**, 1644 (1999).
- ²³E. M. Gershenson, M. E. Gershenson, G. N. Gol'tsman, A. M. Lynl'kin, A. D. Semenov, and A. V. Sergeev, *Sov. Phys. JETP* **70**, 505 (1990).
- ²⁴R. Leoni, F. Mattioli, M. G. Castellano, S. Cibella, P. Carelli, S. Pagano, D. Perez de Lara, M. Ejrnaes, M. P. Lisitskyi, E. Esposito, R. Cristiano, and C. Nappi, *Nucl. Instrum. Methods Phys. Res. A* **559**, 564 (2006).
- ²⁵A. J. Kerman, E. A. Dauler, J. K. W. Yang, K. M. Rosfjord, V. Anant, K. K. Berggren, G. N. Gol'tsman, and B. M. Voronov, *Appl. Phys. Lett.* **90**, 101110 (2007).
- ²⁶Y. P. Gousev, A. D. Semenov, G. N. Gol'tsman, A. V. Sergeev, and E. M. Gershenson, *Physica B* **194-196**, 1355 (1994).
- ²⁷D. F. Santavicca, M. O. Reese, A. B. True, C. A. Schmuttenmaer, and D. E. Prober, *IEEE Trans. Appl. Supercond.* **17**, 412 (2007).
- ²⁸A. J. Annunziata, D. F. Santavicca, L. Frunzio, M. J. Rooks, A. Frydman, and D. E. Prober, *Nanotechnology*, in press (2010).
- ²⁹We report in this paper the total inductance of each device, including the approximately 10 nH of lead inductance. The lead inductance was present in all detection measurements. In later measurements of the inductance of some of these devices in an rf-optimized setup that was not equipped to measure photon detection, the lead inductance was reduced to <1 nH.
- ³⁰N. G. Ptitsina, G. M. Chulkova, K. S. Il'in, A. V. Sergeev, F. S. Pochinkov, E. M. Gershenson, and M. E. Gershenson, *Phys. Rev. B* **56**, 10089 (1997).
- ³¹M. Tinkham, *Introduction to Superconductivity*, 2nd ed. (McGraw-Hill, New York, 1996).
- ³²MATLAB® version 6.5, The MathWorks, Natick, MA, 2007.
- ³³A. Sergeev, A. Semenov, V. Trifonov, B. Karasik, G. Gol'tsman, and E. Gershenson, *J. Supercond.* **7**, 341 (1994).
- ³⁴M. Ejrnaes, A. Casaburi, R. Cristiano, O. Quaranta, S. Marchetti, N. Martucciello, S. Pagano, A. Gaggero, F. Mattioli, R. Leoni, P. Cavalier, and J. C. Villegier, *Appl. Phys. Lett.* **95**, 132503 (2009).
- ³⁵M. Ejrnaes, A. Casaburi, O. Quaranta, S. Marchetti, A. Gaggero, F. Mattioli, R. Leoni, S. Pagano, and R. Cristiano, *Supercond. Sci. Technol.* **22**, 055006 (2009).